Theory of dipole moment reconstruction by attosecond transient absorption spectroscopy

Xiaoxia Wu,[1,2,3,*] Linxuan Zhang,[3,4,*] Shaofeng Zhang,[1,2] and Difa Ye[3,†]
[1]*Institute of Modern Physics, Chinese Academy of Sciences, Lanzhou 730000, China*
[2]*University of Chinese Academy of Sciences, Beijing 100049, China*
[3]*Laboratory of Computational Physics, Institute of Applied Physics and Computational Mathematics, Beijing 100088, China*
[4]*Graduate School, China Academy of Engineering Physics, Beijing 100193, China*

(Received 11 October 2021; revised 2 December 2021; accepted 14 December 2021; published 29 December 2021)

We propose a general procedure for the reconstruction of time-dependent dipole moment via transient absorption spectrum, within the framework of linear response theory. The reconstruction method is demonstrated with two examples: the self-reconstruction of extreme-ultraviolet-light-atom interaction (analytically) and the infrared-dressed helium system (numerically). A correlation coefficient is introduced to quantify the fidelity of the reconstruction, which reaches almost 100% over a wide range of laser parameters and thus indicates the robustness of our reconstruction method. Our theory provides a solid basis for understanding the recent experiment [Phys. Rev. Lett. **121**, 173005 (2018)], explaining when and why the dipole moment can be well reconstructed solely from the absorption spectrum even without exact knowledge of the attosecond probe pulse.

DOI: 10.1103/PhysRevA.104.063121

I. INTRODUCTION

During the past years, the attosecond transient absorption spectroscopy (ATAS) has emerged as a powerful tool for real-time observation of ultrafast dynamics, including strong-field tunneling ionization [1], valence electron motion [2], subcycle ac Stark shift [3,4], and buildup of the Fano resonance [5,6], as well as conical intersection [7,8], to name only a few. In general, this relies on a pump-probe scheme in which the temporal information is mapped onto the delays between two pulses [9–11]. Recently, it was demonstrated in Ref. [12] that with the help of causality (or the Kramers-Kronig relations between absorption and dispersion) [13–16] a single absorption spectrum at a certain time delay is sufficient to restore the full temporal dipole response. This provides a direct access to the quantum beats inside atoms and is beneficial to the understanding of other associated ultrafast phenomena such as the high-order harmonic generation [17]. In a broader perspective, the same method can be also applied to reconstruct the intricate wave packet dynamics in molecules [18] and to follow the attosecond state-resolved carrier motion in materials [19]. One should note, however, the reconstruction theory is accurate only for a $\delta(t)$ pulse, while on the other hand the shortest attosecond pulse currently reported is limited above ∼40 as [20–22]. Therefore, it is natural to ask, for an arbitrary attosecond probe pulse (APP) that is not infinitely short, can the time-dependent dipole moment (TDM) still be reconstructed, and, if yes, how accurate is the reconstruction? These questions stimulate this work.

In this paper, we propose a general theory of TDM reconstruction by ATAS. The key step is to first reconstruct the impulse response function (IRF) that can be retrieved solely from the measurement of the absorption spectrum. Then, if one is also able to accurately measure the APP waveform [23–27], the TDM involved in an arbitrary combined extreme ultraviolet (XUV) and infrared (IR) laser field can be reconstructed straightforwardly by convolution of the IRF and the APP field. Secondly, even when the APP information is lacking, we prove that the TDM is a superposition of the IRF together with a rapidly decaying perturbation that has a lifetime proportional to the APP duration. This explains why and how an APP that has a duration of hundreds of attoseconds can still be applied to robustly reconstruct the long-term behavior of the TDM. We demonstrate our theory first with an example of self-reconstruction of the XUV-atom interaction, in which the atom is described by the Lorentz model and the system is analytically solvable and thus facilitates a clear demonstration of the advantages of our reconstruction method. To further establish the generality of our theory, we then consider an IR-dressed helium atom and a correlation coefficient is introduced to quantify the fidelity of the reconstruction, which indicates that our theory also works successfully in complex systems.

The paper is organized as follows. In Sec. II, a general theory of TDM reconstruction is presented. The main results, including two examples to demonstrate our reconstruction method and the reconstruction fidelity, are presented in Sec. III. Finally, some concluding remarks are made in Sec. IV. Atomic units are used throughout unless otherwise indicated.

II. GENERAL THEORY OF RECONSTRUCTION

In this section, we will present a general theory for the TDM reconstruction. Let us start with the linear response theory that describes the relationship between the TDM and the external laser fields, in the frequency domain

$$\tilde{d}(\omega) = \tilde{\chi}_{\mathrm{IR}}(\omega)\tilde{\mathcal{E}}_X(\omega), \tag{1}$$

*These authors contributed equally to this work.
†ye_difa@iapcm.ac.cn

where $\tilde{\mathcal{E}}_X(\omega)$ is the frequency spectrum of the APP [28] and $\tilde{\chi}_{\rm IR}(\omega)$ represents the electric susceptibility of the system which is modulated by the IR laser field [29,30]. Equivalently, it can be written as a convolution of the impulse [at $\mathcal{E}_X(t) = \mathcal{E}_{X0}\delta(t)$] response function of the IR-dressed system $\chi_{\rm IR}(t)$ and the waveform of the APP $\mathcal{E}_X(t)$, i.e.,

$$d(t) = \frac{1}{\sqrt{2\pi}} \int_0^\infty \chi_{\rm IR}(\tau)\mathcal{E}_X(t-\tau)d\tau. \tag{2}$$

Here, the integration takes only from zero to ∞ due to the causality of a physical response for any material. $d(t)$ is what we would like to reconstruct in the following. In principle, if one knows the electric susceptibility of the system $\tilde{\chi}_{\rm IR}(\omega)$ [or the IRF $\chi_{\rm IR}(t)$] as well as details of the APP [$\mathcal{E}_X(t)$ or $\tilde{\mathcal{E}}_X(\omega)$], then $d(t)$ can be readily determined. However, in most experiments, only the real (Re[$\tilde{\chi}_{\rm IR}(\omega)$], corresponds to dispersion) or imaginary (Im[$\tilde{\chi}_{\rm IR}(\omega)$], corresponds to absorption) part of the complex electric susceptibility is measured. Even so, fortunately, the Kramers-Kronig relations allow one to determine the dispersion with the absorption (or vice versa) and thus to restore the full information of the complex $\tilde{\chi}_{\rm IR}(\omega)$ [13–16]. Below we show how and why the TDM $d(t)$ can be accurately reconstructed with the absorption cross section $\sigma(\omega)(\omega > 0)$.

To this end, we make an even extension of the experimentally measured absorption cross section into the negative frequency domain, i.e.,

$$\sigma(\omega) = \sigma(-\omega) \quad (\omega < 0). \tag{3}$$

Then one can prove that (see Appendix A for details), in the framework of linear response theory, the absorption spectrum measured at an arbitrary APP indeed always gives rise to the IRF [31]

$$\chi_{\rm IR}(t) = \mathcal{F}^{-1}\left[-i\frac{\sigma(\omega)}{2\pi\alpha\omega}\right] \quad (t > 0), \tag{4}$$

and the full TDM $d(t)$ should be reconstructed according to Eq. (2), which requires the temporal information of the APP.

Taking the following XUV laser field, for example,

$$\mathcal{E}_X(t) = \mathcal{E}_{X0}e^{-\lambda|t|}\cos(\omega_X t), \tag{5}$$

we can make some analytical discussions on the reconstruction theory [32]. Here ω_X is the central frequency and $\tau_X = 2\ \ln 2/\lambda$ is the pulse duration, i.e., the full width at half maximum (FWHM). Transforming to the frequency domain, we have

$$\tilde{\mathcal{E}}_X(\omega) = \frac{\mathcal{E}_{X0}}{\sqrt{2\pi}}\left[\frac{\lambda}{\lambda^2+(\omega-\omega_X)^2} + \frac{\lambda}{\lambda^2+(\omega+\omega_X)^2}\right]. \tag{6}$$

We then exploit the fact that in ATAS the pulse duration of the APP ($\sim 1/\lambda$) is much shorter than the typical decoherence time of the system ($\sim 1/\gamma$), i.e., $\lambda \gg \gamma$; therefore, the TDM can be reconstructed by superposition of the IRF and its temporal shifts (see Appendix B for details):

$$d(t) \propto \chi_{\rm IR}(t) + \sum_{n=1}^{\infty} e^{-\frac{n\lambda}{\omega_X}} \cos n\left[\chi_{\rm IR}\left(t+\frac{n}{\omega_X}\right) + \chi_{\rm IR}\left(t-\frac{n}{\omega_X}\right)\right]. \tag{7}$$

It can be seen that the TDM is dominated by the first term for a $\delta(t)$ pulse ($\lambda \to \infty$), while with the increase of the APP duration (decrease of λ) the subsequent other high-order corrections become important. The summation can be truncated at a certain small n such that $n\lambda/\omega_X \approx 1$ due to the exponentially decaying coefficients.

An interesting feature implied in Eq. (7) is that the long-term ($t \gg \tau_X$) behavior of the TDM is proportional to and can be represented by the IRF, if the amplitude of the dipole oscillation is slowly modulated within the time scale of the APP duration. This can be verified by separating the slow and fast variables of the IRF as $\chi_{\rm IR}(t) = f(t)\sin(\omega_0 t + \phi)$, where $f(t)$ is a slowly varying modulation function, i.e., $df/dt \ll \lambda$. Then, according to the exponentially decaying coefficients we only need to take the first few n into account, and in such case for every small n, $f(t \pm n/\omega_X) \approx f(t \pm 1/\lambda) \approx f(t)$, so that $\chi_{\rm IR}(t + n/\omega_X) + \chi_{\rm IR}(t - n/\omega_X) \approx 2f(t)\cos(n\omega_0/\omega_X)\sin(\omega_0 t + \phi) \propto \chi_{\rm IR}(t)$, indicating that $d(t)$ is also proportional to $\chi_{\rm IR}(t)$. As will be discussed in more details in Sec. III, the above approximations are satisfied in many typical cases of ATAS, e.g., (i) for XUV-atom interaction, $f(t) \sim e^{-\gamma t}$; therefore, $df/dt \ll \lambda$ means $\gamma \ll \lambda$, which is the case in ATAS; (ii) for an IR-dressed atom, $f(t) \sim \cos(\Omega t)$; therefore, $df/dt \ll \lambda$ requires $\Omega \ll \lambda$, where Ω is the Rabi frequency [33].

Up to this point, we have developed a general procedure for the TDM reconstruction: by measuring the absorption spectrum, we can use Eq. (4) to calculate the IRF or IR-dressed electric susceptibility; then if we are also able to accurately measure the APP waveform, the TDM can be obtained from Eq. (1) or Eq. (2). When the XUV laser field is not exactly known, we can use Eq. (7) to make a rough estimation of the TDM, which depends only on some key laser parameters. Finally, even if the APP is totally unknown, one can still use Eq. (4) to retrieve the long-term behavior of the TDM.

III. RESULTS AND DISCUSSIONS

A. Enlightening example: Self-reconstruction

As a demonstration of our reconstruction theory, we first consider the simple case of a single resonance $\omega = \omega_0$ without the IR dressed field. The electric susceptibility is described by the Lorentz model as known in textbooks [34],

$$\tilde{\chi}_0(\omega) = \frac{\omega_p^2}{\omega_0^2 - \omega^2 + i\gamma\omega}, \tag{8}$$

where ω_p is the plasma frequency. The IRF can be evaluated by contour integration [refer to Eq. (A4) of Appendix A], which gives rise to

$$\chi_0(t) = \sqrt{2\pi}\omega_p^2 e^{-\gamma t/2}\frac{\sin \nu_0 t}{\nu_0}\theta(t), \tag{9}$$

where $\nu_0 = \sqrt{\omega_0^2 - \gamma^2/4}$ and $\theta(t)$ is the step function indicating the causality. Substituting Eqs. (6) and (8) into Eq. (1) and then performing the inverse Fourier transformation, we can calculate the full dipole response analytically. Here, the Fourier transformation can be evaluated by contour

integration. The integrand has six poles in the complex-ω plane: two poles $z_\pm = \pm\nu_0 + i\gamma/2$ associated to the bare atomic electric susceptibility [red full circles in Fig. 1(a), closer to the real axis] and another four poles $z_1 = \omega_X + i\lambda$, $z_2 = -\omega_X + i\lambda$, $z_3 = -\omega_X - i\lambda$, and $z_4 = \omega_X - i\lambda$ introduced due to the finite duration of the APP [black full circles in Fig. 1(a), far away from the real axis]. The poles z_{1-4} will disappear for a $\delta(t)$-probe pulse. The contour is closed in the upper (lower) half-plane for $t > 0$ ($t < 0$), respectively. Then, according to Cauchy's theorem, we get

$$d(t) = \begin{cases} \omega_p^2 \mathcal{E}_{X0}\left[\lambda\, e^{-\gamma t/2}\left(\alpha_1 \dfrac{\sin\nu_0 t}{\nu_0} + \beta_1 \dfrac{\cos\nu_0 t}{\nu_0}\right) + e^{-\lambda t}(\alpha_2 \cos\omega_X t - \beta_2 \sin\omega_X t)\right], & t > 0, \\ \omega_p^2 \mathcal{E}_{X0} e^{\lambda t}[\alpha_3 \cos\omega_X t - \beta_3 \sin\omega_X t], & t < 0, \end{cases} \tag{10}$$

where $\alpha_1 = \frac{a_+}{a_+^2+b_+^2} + \frac{a_-}{a_-^2+b_-^2}$, $\beta_1 = \frac{-b_+}{a_+^2+b_+^2} + \frac{-b_-}{a_-^2+b_-^2}$, $\alpha_2 = \frac{c_+}{c_+^2+d_+^2}$, $\beta_2 = \frac{-d_+}{c_+^2+d_+^2}$, $\alpha_3 = \frac{c_-}{c_-^2+d_-^2}$, and $\beta_3 = \frac{-d_-}{c_-^2+d_-^2}$, with $a_\pm = (\nu_0 \pm \omega_0)^2 + \lambda^2 - \gamma^2/4$, $b_\pm = \gamma(\nu_0 \pm \omega_0)$, $c_\pm = \lambda(\lambda \mp \gamma)$, and $d_\pm = \omega_0(\gamma \mp 2\lambda)$. From these expressions we see that, even for this rather simple case, the TDM differs from the IRF in many aspects, including a phase-shifted term [second term in the first line of Eq. (10)] and another two decaying terms [last two terms in the first line of Eq. (10)], as well as the $t < 0$ component. However, all these differences disappear if $\lambda \gg \gamma$, for which $e^{-\lambda t}$ decays much faster than $e^{-\gamma t/2}$ and $\alpha_1 \gg \beta_1$; therefore, $d(t)$ is roughly proportional to $\chi_0(t)$ besides a rapidly decaying perturbation that fades away as $t \to \infty$ [see Fig. 1(b)]. This provides an enlightening example to explain why even an APP that is not infinitely short is capable of robustly reconstructing the long-term behavior of the TDM.

Figure 1(c) shows a typical run of the dipole-moment reconstruction, comparing the original TDM (open circles) with those reconstructed based on Eq. (2) (blue solid curve) and Eq. (7) (full squares). It can be seen that our theory is able to accurately reconstruct the TDM, including the $t < 0$ component, even when the APP is relatively long, e.g., of the order of hundreds of attoseconds.

B. Application to IR dressed system

To further demonstrate the validity of our reconstruction theory, we now consider the ATAS of an IR-dressed helium atom [35,36]. We focus on the singly excited states and exploit the single-active-electron (SAE) approximation [37–43]; for two-electron full-dimensional treatment, see, e.g., Refs. [44–47]. In specific, the system under study is described with a three-level model composed of the $1s^2$ ($|g\rangle$), $1s2p$ ($|a\rangle$), and $1s2s$ ($|f\rangle$) states of He, whose dynamics is governed by the following discrete Schrödinger equations:

$$i\frac{d}{dt}\begin{pmatrix} C_g \\ C_a \\ C_f \end{pmatrix} = \begin{pmatrix} 0 & H_{ga} & 0 \\ H_{ag} & 0 & H_{af} \\ 0 & H_{fa} & 0 \end{pmatrix}\begin{pmatrix} C_g \\ C_a \\ C_f \end{pmatrix}, \tag{11}$$

where C_g, C_a, and C_f are the probability amplitudes of the corresponding states; H_{ga}, H_{ag}, H_{af}, and H_{fa} are the transition matrix elements, taking the form $H_{ga} = \mu_{ga}\mathcal{E}_X(t)e^{-i\Delta_{ga}t}$, $H_{af} = \mu_{af}\mathcal{E}_{\rm IR}(t,\tau)e^{-i\Delta_{af}t}$, $H_{ag} = H_{ga}^*$, and $H_{fa} = H_{af}^*$. The energy levels and dipole transition matrix elements can be determined from first principles [48,49], i.e., $\Delta_{ga} = E_a - E_g = 21.057$ eV, $\Delta_{af} = E_f - E_a = -0.82$ eV, $\mu_{ga} = \langle g|z|a\rangle = 0.34$ a.u., and $\mu_{af} = \langle a|z|f\rangle = 2.72$ a.u. The APP is described by Eq. (5), while the IR field takes the form $\mathcal{E}_{\rm IR}(t,\tau) = \mathcal{E}_0\mathscr{A}(t-\tau)\cos[\omega_{\rm IR}(t-\tau)]$, where $\mathscr{A}(t-\tau) = \cos^2[\omega_{\rm IR}(t-\tau)/2N]$($|t-\tau| \leqslant N\pi/\omega_{\rm IR}$) is the pulse envelope with N the total number of optical cycles. The Schrödinger equations for the three-level system are solved numerically by employing the standard forth- and fifth-order Runge-Kutta algorithm, which gives the original TDM to be reconstructed. We then calculated the absorption spectrum with [50]

$$\sigma(\omega) = -4\pi\alpha\omega\,\mathrm{Im}\left[\frac{\tilde{d}(\omega)}{\tilde{\mathcal{E}}_X(\omega)}\right] \quad (\omega > 0) \tag{12}$$

to mimic the experimentally measured one and demonstrate the subsequent reconstruction procedure.

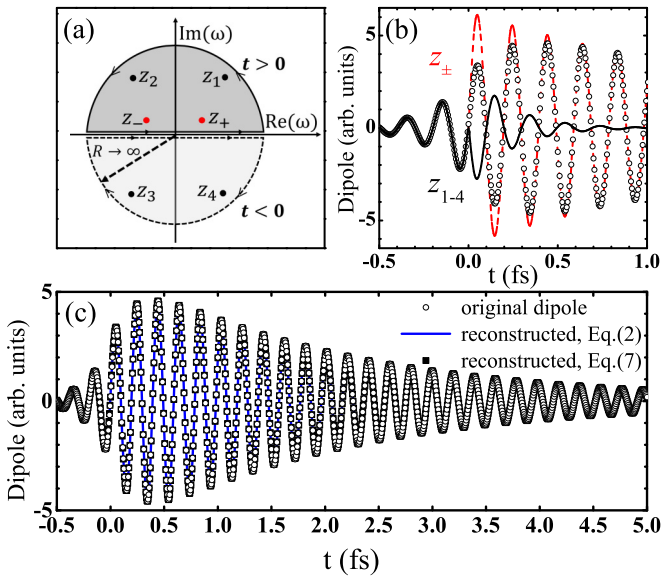

FIG. 1. (a) Illustration of the poles' location and the path of contour integration in calculating the TDM. (b) The full TDM is decomposed into slow and fast decaying terms, owing to the bare atomic electric susceptibility (red dashed curve) and induced by the finite range of the APP duration (black solid curve), respectively. (c) Comparison between the original TDM (open circles) and the reconstructed ones based on Eq. (2) (blue solid curve) and Eq. (7) (full squares), respectively. The laser parameters are $I_X = 10^{10}$ W/cm^2, $\tau_X = 300$ as, and $\omega_X = 21$ eV. For clear visualization, we assume the decoherence time to be $1/\gamma = 1$ fs. In practice, the decoherence time can be much longer and the reconstruction is even better.

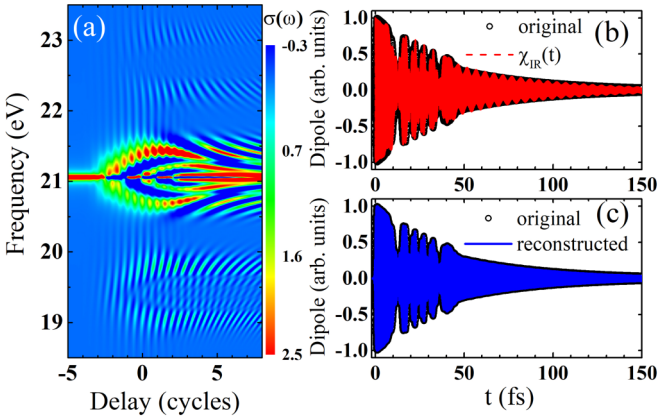

FIG. 2. (a) Typical attosecond transient absorption spectrum. The APP field is the same as that in Fig. 1, while the IR laser parameters are $I_{\rm IR} = 5$ TW/cm^2, $\omega_{\rm IR} = 0.82$ eV, and $N = 10$. The decoherence time is assumed to be $1/\gamma = 50$ fs. Comparison of the IRF (red dashed curve) and the reconstructed TDM (blue solid curve) with the original dipole moment (scatters) are demonstrated in (b) and (c), respectively

A typical calculated ATAS is shown in Fig. 2(a), where the time delay is positive (negative) if the IR pulse arrives after (before) the XUV pulse. Without loss of generality, we choose the absorption spectrum at the delay of five optical cycles to reconstruct the TDM. As can be seen from Fig. 2(b) the IRF $\chi_{\rm IR}(t)$ has some fine structures different from the original TDM, while the reconstruction based on Eq. (2) is overall excellent [Fig. 2(c)].

Inspecting more closely, we zoom in on the TDMs around the time zero (beginning of the dipole oscillation), as well as at the vicinity of 12 fs (long-term oscillation). The results are shown in Fig. 3 at four different τ_X. It can be seen that, when the XUV pulse is a δ-kick [$\tau_X = 0$, Fig. 3(a)], the reconstructed TDM as well as $\chi_{\rm IR}(t)$ fully reproduces the original TDM over the whole time domain, as one might expect. For

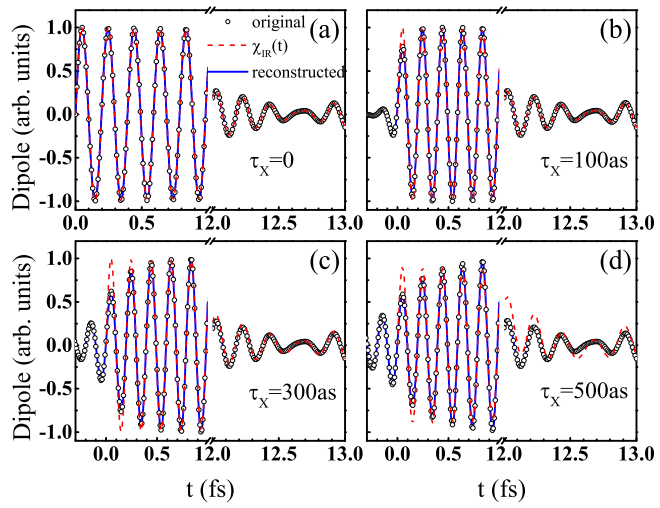

FIG. 3. Reconstructed TDMs as compared with the original ones when the APP has a duration of 0 (a), 100 (b), 300 (c), and 500 as (d), respectively. Other laser parameters are the same as those in Fig. 2.

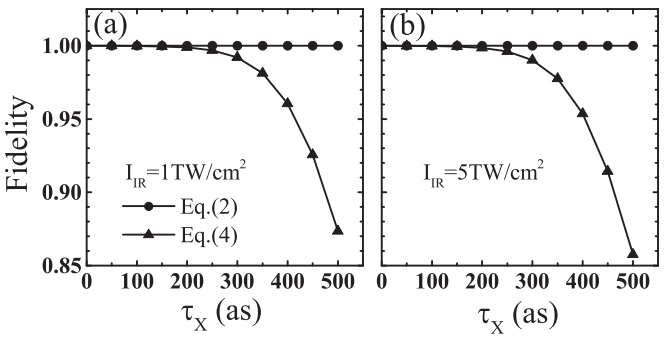

FIG. 4. Fidelity of the TDM reconstruction as a function of the XUV pulse duration at different IR laser intensities $I_{\rm IR} = 1$ TW/cm^2 (a) and 5 TW/cm^2 (b). Other laser parameters are the same as those in Fig. 2.

an APP with finite pulse duration [Figs. 3(b)–3(d)], the dipole oscillation starts slightly before the time zero. Therefore, the IRF $\chi_{\rm IR}(t)$ does not well reproduce the original TDM within the first few hundreds of attoseconds. It even fails to predict the long-term behavior of the TDM when the APP duration increases up to 500 as [Fig. 3(d)]. In all cases, by comparison, the reconstruction method based on Eq. (2) (blue curves) always works successfully.

C. Fidelity of the reconstruction

To quantify the fidelity of the reconstruction, we introduce the following correlation coefficient between two variables [51]:

$$\mathscr{R}(X,Y) = \frac{\mathrm{Cov}(X,Y)}{\sqrt{\mathrm{Var}[X]\,\mathrm{Var}[Y]}}, \tag{13}$$

where $\mathrm{Var}[X] = \overline{(X-\overline{X})^2}$ describes the variance of X and $\mathrm{Cov}(X,Y) = \overline{(X-\overline{X})(Y-\overline{Y})}$ represents the covariance between X and Y. In our calculations, X and Y denote the reconstructed TDM and the original one, respectively. Therefore, $\mathscr{R} = 1$ indicates that the TDM is 100% reconstructed.

As one can see from Fig. 4, although both $\chi_{\rm IR}(t)$ and $d(t)$ reconstructed with Eq. (4) and Eq. (2) can faithfully reproduce the original TDM, the latter is a better choice, almost reaching 100% fidelity. In general, a shorter XUV pulse can be applied to reconstruct the TDM with higher reliability as one can expect. Meanwhile, with the increase of the IR laser intensity, strong-field and multiphoton effects might come into play; therefore, the TDM becomes more difficult to be reconstructed. For those cases with lower reconstruction fidelity, the deviation is mainly caused during the first hundreds of attoseconds and at the positions that the amplitude of the dipole oscillation is modulated close to zero due to Rabi flopping.

IV. CONCLUSION

In summary, we have provided a general recipe for the time-dependent dipole moment reconstruction by attosecond transient absorption spectrum, either with or without additional measurement of the attosecond probe pulse waveform or frequency spectrum. We have demonstrated that the

reconstruction method can reach almost 100% fidelity as far as the APP duration is sufficiently short and the linear response theory is valid. The underlying mechanisms have been revealed by perturbation theory in the time domain and complemented by complex analysis in the frequency domain, both indicating that the difference between the original dipole response and the reconstructed one is significantly reduced with the shrink of the APP duration. The reconstruction theory does not necessary rely on detailed information of the physical system that is under investigation or even not on the probe field. It is thus rather general and could be extended to other types of transient absorption spectroscopy.

ACKNOWLEDGMENTS

We are grateful to Dr. L. Xu for valuable discussions. This work was supported by the National Key Research and Development Program of China (No. 2017YFA0402300) and the National Natural Science Foundation of China (Grants No. 12174034, No. 11822401, and No. 11775030).

APPENDIX A: DERIVATION OF EQ. (4)

In this section, we make a detailed derivation of Eq. (4) in the main text, which is valid under the linear response assumption of Eq. (1); thus

$$\mathcal{F}^{-1}\left[-i\frac{\sigma(\omega)}{2\pi\alpha\omega}\right]=\mathcal{F}^{-1}\{2i\,\mathrm{Im}[\tilde{\chi}_{\mathrm{IR}}(\omega)]\}$$
$$=\mathcal{F}^{-1}[\tilde{\chi}_{\mathrm{IR}}(\omega)-\tilde{\chi}^{*}_{\mathrm{IR}}(\omega)]. \quad \text{(A1)}$$

Here, $\tilde{\chi}_{\mathrm{IR}}(\omega)$ only has poles in the upper half of the complex ω plane as restricted by the principle of causality. We mark the poles of first order as $Z_1, Z_2, \ldots, Z_n$ and define

$$f(\omega)=\frac{1}{\tilde{\chi}_{\mathrm{IR}}(\omega)}=g(\omega)(\omega-Z_1)(\omega-Z_2)\ldots(\omega-Z_n). \quad \text{(A2)}$$

The first part in Eq. (A1) is nothing but $\chi_{\mathrm{IR}}(t)$,

$$\chi_{\mathrm{IR}}(t)=\mathcal{F}^{-1}[\tilde{\chi}_{\mathrm{IR}}(\omega)]=\frac{1}{\sqrt{2\pi}}\int_{-\infty}^{\infty}\frac{1}{f(\omega)}e^{i\omega t}d\omega, \quad \text{(A3)}$$

which can be evaluated by the contour integration. For $t>0$, the contour is closed in the upper half ω plane and the integral is given by $2\pi i$ times the residues at the poles; hence we have

$$\chi_{\mathrm{IR}}(t)=\sqrt{2\pi}i\sum_{k=1}^{n}\frac{e^{iZ_k t}}{g(Z_k)\prod_{j\neq k}(Z_k-Z_j)} \quad (t>0). \quad \text{(A4)}$$

Similarly, $\mathcal{F}^{-1}[\tilde{\chi}^{*}_{\mathrm{IR}}(\omega)]$ can also be calculated by the contour integration as follows:

$$\mathcal{F}^{-1}[\tilde{\chi}^{*}_{\mathrm{IR}}(\omega)]=\frac{1}{\sqrt{2\pi}}\int_{-\infty}^{\infty}\frac{1}{f^{*}(\omega)}e^{i\omega t}d\omega$$
$$=\frac{1}{\sqrt{2\pi}}\left[\int_{-\infty}^{\infty}\frac{1}{f(\omega)}e^{-i\omega t}d\omega\right]^{*}. \quad \text{(A5)}$$

The difference is that, for $t>0$, the contour should now be closed in the lower half ω plane due to the minus sign in the exponent, whereas all the poles are in the upper half ω plane. It is thus clear that $\mathcal{F}^{-1}[\tilde{\chi}^{*}_{\mathrm{IR}}(\omega)]=0$ when $t>0$. Substituting it back into Eq. (A1), one finally arrives at Eq. (4).

APPENDIX B: DERIVATION OF EQ. (7)

According to Eq. (1), the TDM is determined by the following inverse Fourier transformation:

$$d(t)=\frac{1}{\sqrt{2\pi}}\int_{-\infty}^{\infty}\tilde{\chi}_{\mathrm{IR}}(\omega)\tilde{\mathcal{E}}_X(\omega)e^{i\omega t}d\omega. \quad \text{(B1)}$$

For a long-lived state, $\tilde{\chi}_{\mathrm{IR}}(\omega)$ is much narrower than $\tilde{\mathcal{E}}_X(\omega)$ since $\gamma\ll\lambda$; therefore, we only need to care about a fairly narrow range $(-\omega_0,\omega_0)$. In this case, we make a periodic extension of $\tilde{\mathcal{E}}_X(\omega)$ and cast Eq. (6) into a series of trigonometric functions

$$\tilde{\mathcal{E}}_X(\omega)\approx\frac{a_0}{2}+\sum_{n=1}^{\infty}\left[a_n\cos\left(\frac{n\omega}{\omega_X}\right)+b_n\sin\left(\frac{n\omega}{\omega_X}\right)\right], \quad \text{(B2)}$$

where the coefficients are determined by

$$a_0=\frac{1}{\pi\omega_X}\int_{-\infty}^{\infty}\tilde{\mathcal{E}}_X(\omega)d\omega,$$
$$a_n=\frac{1}{\pi\omega_X}\int_{-\infty}^{\infty}\tilde{\mathcal{E}}_X(\omega)\cos\left(\frac{n\omega}{\omega_X}\right)d\omega,$$
$$b_n=\frac{1}{\pi\omega_X}\int_{-\infty}^{\infty}\tilde{\mathcal{E}}_X(\omega)\sin\left(\frac{n\omega}{\omega_X}\right)d\omega. \quad \text{(B3)}$$

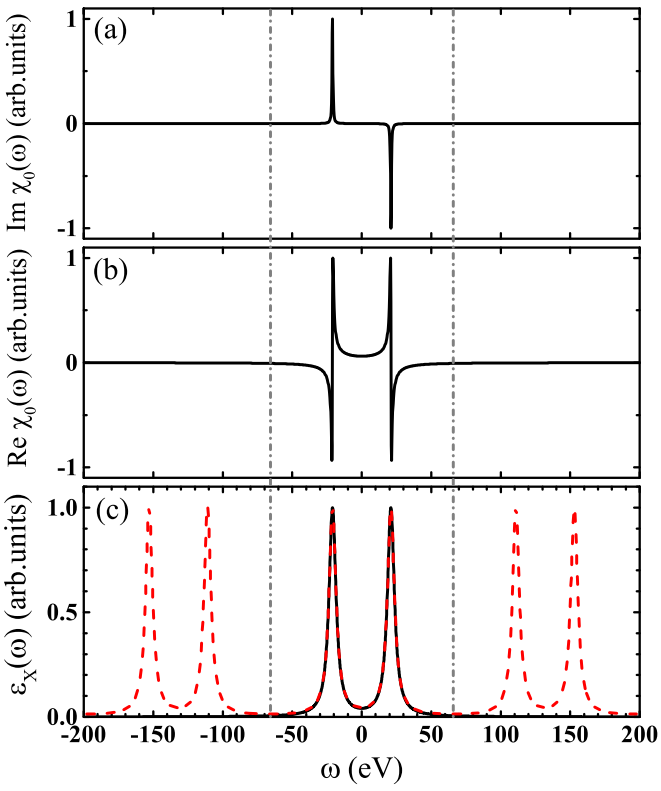

FIG. 5. Illustration of the imaginary (a) and real (b) parts of the susceptibility together with the frequency spectrum of the APP. The solid and dashed curves in (c) represent the original spectrum [Eq. (6)] and its periodic extension [Eq. (B6)], respectively. The dashed-dotted lines show the boundaries of $\pm\pi\omega_X$, within which the two spectra in (c) are almost identical; therefore, the approximation of Eq. (7) is valid.

For the APP [Eq. (6)] adopted in this paper, the above integrations can be calculated analytically according to Cauchy's theorem, for example,

$$\begin{aligned} a_n &= \frac{\mathcal{E}_{X0}}{(2\pi)^{3/2}\omega_X}\int_{-\infty}^{\infty}(\Xi_{++}+\Xi_{+-}+\Xi_{-+}+\Xi_{--})d\omega \\ &= \frac{i\mathcal{E}_{X0}}{\sqrt{2\pi}\,\omega_X}[\mathrm{Res}\,\Xi_{++}|_{\omega=i\lambda-\omega_X}-\mathrm{Res}\,\Xi_{+-}|_{\omega=-i\lambda-\omega_X} \\ &\quad +\mathrm{Res}\,\Xi_{-+}|_{\omega=i\lambda+\omega_X}-\mathrm{Res}\,\Xi_{--}|_{\omega=-i\lambda+\omega_X}] \\ &= \frac{2\mathcal{E}_{X0}}{\sqrt{2\pi}\,\omega_X}e^{-\frac{n\lambda}{\omega_X}}\cos n, \end{aligned} \tag{B4}$$

where

$$\Xi_{++} = \frac{\lambda}{\lambda^2+(\omega+\omega_X)^2}e^{\frac{in\omega}{\omega_X}},$$

$$\Xi_{+-} = \frac{\lambda}{\lambda^2+(\omega+\omega_X)^2}e^{-\frac{in\omega}{\omega_X}},$$

$$\Xi_{-+} = \frac{\lambda}{\lambda^2+(\omega-\omega_X)^2}e^{\frac{in\omega}{\omega_X}},$$

$$\Xi_{--} = \frac{\lambda}{\lambda^2+(\omega-\omega_X)^2}e^{-\frac{in\omega}{\omega_X}}. \tag{B5}$$

Similarly, we have $a_0 = 2\mathcal{E}_{X0}/\sqrt{2\pi}\omega_X$ and $b_n = 0$; therefore,

$$\tilde{\mathcal{E}}_X(\omega) \approx \frac{\mathcal{E}_{X0}}{\sqrt{2\pi}\,\omega_X}\left[1+2\sum_{n=1}^{\infty}e^{-\frac{n\lambda}{\omega_X}}\cos n\,\cos\left(\frac{n\omega}{\omega_X}\right)\right]. \tag{B6}$$

As can be seen from Fig. 5, this approximated expansion is in general very good within the interval of $[-\pi\omega_X, \pi\omega_X]$. Consequently, when calculating the TDM with inverse Fourier transform, we can replace Eq. (6) with Eq. (B6). Substituting Eq. (B6) back into Eq. (B1), we can finally obtain Eq. (7).

[1] M. Sabbar, H. Timmers, Y.-J. Chen, A. K. Pymer, Z.-H. Loh, S. G. Sayres, S. Pabst, R. Santra, and S. R. Leone, Nat. Phys. **13**, 472 (2017).

[2] E. Goulielmakis *et al.*, Nature (London) **466**, 739 (2010).

[3] M. Chini, B. Z. Zhao, H. Wang, Y. Cheng, S. X. Hu, and Z. H. Chang, Phys. Rev. Lett. **109**, 073601 (2012).

[4] K. Mi, W. Cao, H. Xu, Y. Mo, Z. Yang, P. Lan, Q. Zhang, and P. Lu, Phys. Rev. Appl. **13**, 014032 (2020).

[5] A. Kaldun, A. Blättermann, V. Stooß, S. Donsa, H. Wei, R. Pazourek, S. Nagele, C. Ott, C. D. Lin, J. Burgdörfer, and T. Pfeifer, Science **354**, 738 (2016).

[6] Y. He, Z. Liu, N. Xue, C. Ott, T. Pfeifer, A. N. Pfeiffer, and B. Hu, Phys. Rev. A **103**, L041102 (2021).

[7] J. E. Bækhøj, C. Lévêque, and L. B. Madsen, Phys. Rev. Lett. **121**, 023203 (2018).

[8] K. S. Zinchenko, F. Ardana-Lamas, I. Seidu, S. P. Neville, J. van der Veen, V. U. Lanfaloni, M. S. Schuurman, and H. J. Wörner, Science **371**, 489 (2021).

[9] L. Gallmann, J. Herrmann, R. Locher, M. Sabbar, A. Ludwig, M. Lucchini, and U. Keller, Mol. Phys. **111**, 2243 (2013).

[10] A. R. Beck, D. M. Neumark, and S. R. Leone, Chem. Phys. Lett. **624**, 119 (2015).

[11] M. Wu, S. Chen, S. Camp, K. J. Schafer, and M. B. Gaarde, J. Phys. B **49**, 062003 (2016).

[12] V. Stooß, S. M. Cavaletto, S. Donsa, A. Blättermann, P. Birk, C. H. Keitel, I. Březinová, J. Burgdörfer, C. Ott, and T. Pfeifer, Phys. Rev. Lett. **121**, 173005 (2018).

[13] R. de L. Kronig, J. Opt. Soc. Am. **12**, 547 (1926).

[14] H. A. Kramers, Atti Congr. Int. Fis. **2**, 545 (1927).

[15] R. Kubo, J. Phys. Soc. Jpn. **12**, 570 (1957).

[16] C. W. Peterson and B. W. Knight, J. Opt. Soc. Am. **63**, 1238 (1973).

[17] M. Protopapas, C. H. Keitel, and P. L. Knight, Rep. Prog. Phys. **60**, 398 (1997).

[18] Y. Cheng, M. Chini, X. Wang, A. González-Castrillo, A. Palacios, L. Argenti, F. Martín, and Z. Chang, Phys. Rev. A **94**, 023403 (2016).

[19] M. Volkov, S. A. Sato, F. Schlaepfer, L. Kasmi, N. Hartmann, M. Lucchini, L. Gallmann, A. Rubio, and U. Keller, Nat. Phys. **15**, 1145 (2019).

[20] K. Zhao, Q. Zhang, M. Chini, Y. Wu, X. W. Wang, and Z. H. Chang, Opt. Lett. **37**, 3891 (2012).

[21] J. Li, X. M. Ren, Y. C. Yin, K. Zhao, A. Chew, Y. Cheng, E. Cunningham, Y. Wang, S. Y. Hu, Y. Wu, M. Chini, and Z. H. Chang, Nat. Commun. **8**, 186 (2017).

[22] T. Gaumnitz, A. Jain, Y. Pertot, M. Huppert, I. Jordan, F. Ardana-Lamas, and H. J. Wörner, Opt. Express **25**, 027506 (2017).

[23] P. M. Paul, E. S. Toma, P. Breger, G. Mullot, F. Augé, Ph. Balcou, H. G. Muller, and P. Agostini, Science **292**, 1689 (2001).

[24] M. Drescher, M. Hentschel, R. Kienberger, G. Tempea, C. Spielmann, G. A. Reider, P. B. Corkum, and F. Krausz, Science **291**, 1923 (2001).

[25] J. Itatani, F. Quéré, G. L. Yudin, M. Yu. Ivanov, F. Krausz, and P. B. Corkum, Phys. Rev. Lett. **88**, 173903 (2002).

[26] Y. Mairesse and F. Quéré, Phys. Rev. A **71**, 011401(R) (2005).

[27] A. Kosuge, T. Sekikawa, X. Zhou, T. Kanai, S. Adachi, and S. Watanabe, Phys. Rev. Lett. **97**, 263901 (2006).

[28] The overhead tilde indicates Fourier transformation into the frequency domain. Throughout this paper, we have adopted the Fourier transformation convention $\tilde{f}(\omega) = \frac{1}{\sqrt{2\pi}}\int_{-\infty}^{\infty} f(t)e^{-i\omega t}dt$ and $f(t) = \frac{1}{\sqrt{2\pi}}\int_{-\infty}^{\infty}\tilde{f}(\omega)e^{i\omega t}d\omega$.

[29] C. Ott, A. Kaldun, P. Raith, K. Meyer, M. Laux, J. Evers, C. H. Keitel, C. H. Greene, and T. Pfeifer, Science **340**, 716 (2013).

[30] A. Kaldun, C. Ott, A. Blättermann, M. Laux, K. Meyer, T. Ding, A. Fischer, and T. Pfeifer, Phys. Rev. Lett. **112**, 103001 (2014).

[31] The even extension of the absorption cross section ensures that the reconstructed $\chi_{\mathrm{IR}}(t)$ is purely real.

[32] Here we have adopted a specific envelope for the APP to facilitate our following analytical discussions. We would like to emphasize that the physical picture we present does not depend on the exact form of the field. We also note that the double-exponential envelope function has been adopted in some other literatures; see, e.g., C. D. Lin *et al.*, *Attosecond and*

Strong-Field Physics: Principles and Applications (Cambridge University Press, Cambridge, England, 2018), p. 359.
[33] I. I. Rabi, Phys. Rev. **51**, 652 (1937).
[34] Due to the Fourier transformation convention adopted in this paper, the electric susceptibility has a sign different from the formulas in some textbooks; see, e.g., J. D. Jackson, *Classical Electrodynamics*, 3rd ed. (Wiley, New York, 1999). Note that the location of the poles could be different too.
[35] Z. Q. Yang, D. F. Ye, T. Ding, T. Pfeifer, and L. B. Fu, Phys. Rev. A **91**, 013414 (2015).
[36] X. X. Wu, Z. Q. Yang, S. F. Zhang, X. W. Ma, J. Liu, and D. F. Ye, Phys. Rev. A **103**, L061102 (2021).
[37] A. N. Pfeiffer and S. R. Leone, Phys. Rev. A **85**, 053422 (2012).
[38] S. Chen, M. Wu, M. B. Gaarde, and K. J. Schafer, Phys. Rev. A **87**, 033408 (2013).
[39] M. Murakami and S.-I. Chu, Phys. Rev. A **88**, 043428 (2013).
[40] M. Chini, X. Wang, Y. Cheng, and Z. Chang, J. Phys. B **47**, 124009 (2014).
[41] W. Dong, Y. Li, X. Wang, J. Yuan, and Z. Zhao, Phys. Rev. A **92**, 033412 (2015).
[42] H. W. Zhao, C. D. Liu, Y. H. Zheng, Z. N. Zeng, and R. X. Li, Opt. Express **25**, 7707 (2017).
[43] G. Yuan, S. Jiang, Z. Wang, W. Hua, C. Yu, C. Jin, and R. Lu, Struct. Dyn. **6**, 054102 (2019).
[44] S. X. Hu and L. A. Collins, Phys. Rev. Lett. **96**, 073004 (2006).
[45] T. Morishita, S. Watanabe, and C. D. Lin, Phys. Rev. Lett. **98**, 083003 (2007).
[46] S. X. Hu, Phys. Rev. Lett. **111**, 123003 (2013).
[47] L. Argenti, Á. Jiménez-Galán, C. Marante, C. Ott, T. Pfeifer, and F. Martín, Phys. Rev. A **91**, 061403(R) (2015).
[48] X. M. Tong and S. I. Chu, Chem. Phys. **217**, 119 (1997).
[49] X. M. Tong and C. D. Lin, J. Phys. B **38**, 2593 (2005).
[50] M. B. Gaarde, C. Buth, J. L. Tate, and K. J. Schafer, Phys. Rev. A **83**, 013419 (2011).
[51] J. A. Rice, *Mathematical Statistics and Data Analysis*, 3rd ed. (University of California, Berkeley, 2007).